

1-1-2012

## Different radiolabelling methods alter the pharmacokinetic and biodistribution properties of Plasminogen Activator Inhibitor Type 2 (PAI-2) forms

Marie Ranson  
*University of Wollongong, [mranson@uow.edu.au](mailto:mranson@uow.edu.au)*

Paula Berghofer  
*ANSTO*


Kara L. Vine  
*University of Wollongong, [kara@uow.edu.au](mailto:kara@uow.edu.au)*

Ivan Greguric  
*University of Wollongong*

Rachael Shepherd  
*ANSTO*

*See next page for additional authors*

Follow this and additional works at: <https://ro.uow.edu.au/scipapers>

 Part of the [Life Sciences Commons](#), [Physical Sciences and Mathematics Commons](#), and the [Social and Behavioral Sciences Commons](#)

---

### Recommended Citation

Ranson, Marie; Berghofer, Paula; Vine, Kara L.; Greguric, Ivan; Shepherd, Rachael; and Katsifis, Andrew: Different radiolabelling methods alter the pharmacokinetic and biodistribution properties of Plasminogen Activator Inhibitor Type 2 (PAI-2) forms 2012, 833-839.  
<https://ro.uow.edu.au/scipapers/4268>

---

## Different radiolabelling methods alter the pharmacokinetic and biodistribution properties of Plasminogen Activator Inhibitor Type 2 (PAI-2) forms

### Abstract

**Introduction:** Tumour-associated urokinase plasminogen activator (uPA) is a critical marker of invasion and metastasis, and it is recognised as having strong prognostic relevance as well as being a therapeutic target. The specific uPA inhibitor plasminogen activator inhibitor type-2 (PAI-2, SerpinB2) specifically targets cell bound uPA and is internalised. Furthermore, preclinical studies have established the “proof-of-principle” of uPA-targeting by PAI-2-cytotoxin conjugates in human carcinoma models. However, these studies also suggest that PAI-2 is rapidly cleared via the renal system with low total dose reaching the tumour. In this study, a comparative single photon emission computed tomography (SPECT) and biodistribution (BD) analysis of different forms of PAI-2 labelled with the radioisotopes iodine-123 (<sup>123</sup>I) and technetium-99m (<sup>99m</sup>Tc) was undertaken. **Methods:** The pharmacokinetic (PK) properties and BD of wild-type,  $\Delta$ CD-loop and PEGylated  $\Delta$ CD-loop PAI-2 labelled with the commonly used diagnostic SPECT radioisotopes <sup>99m</sup>Tc or <sup>123</sup>I were compared in mouse models of human prostate carcinoma. Whole body SPECT imaging was also performed. **Results:** Both wild-type or the shorter but active  $\Delta$ CD-loop form of PAI-2 <sup>123</sup>I-labelled indirectly via conjugation to free amine groups (termed <sup>123</sup>I-Bn-PAI-2) exhibited low tumour uptake, rapid excretion and similar PK profiles. Preliminary studies with a short branched-chain PEGylated <sup>123</sup>I-Bn-PAI-2  $\Delta$ CD-loop indicated an increase in blood retention time and tumour uptake. All <sup>123</sup>I-Bn-labelled radiotracers were largely excreted through the kidneys. By comparison, both wild-type <sup>123</sup>I-PAI-2 (labelled directly via tyrosine residues) and <sup>99m</sup>Tc-PAI-2 displayed different PK/BD patterns compared to <sup>123</sup>I-Bn- PAI-2, suggesting greater liver based catabolism and thus slower elimination. SPECT imaging mimicked the BD results of all radiotracers. **Conclusion:** The different labelling methods gave distinct PAI-2 BD and tumour uptake profiles, with radioiodination resulting in the best non-tumour organ clearance profiles. Preliminary analyses with short branched-chain PEGylated <sup>123</sup>I-Bn-PAI-2  $\Delta$ CD-loop suggest that further investigations with other PEGylation reagents are required to optimise this approach for tumour imaging. These findings impact on the use of PAI-2 for drug delivery and/or diagnostic development.

### Keywords

plasminogen, activator, inhibitor, type, 2, pai, forms, methods, alter, pharmacokinetic, different, biodistribution, radiolabelling, properties, CMMB

### Disciplines

Life Sciences | Physical Sciences and Mathematics | Social and Behavioral Sciences

### Publication Details

Ranson, M., Berghofer, P., Vine, K. L., Greguric, I., Shepherd, R. & Katsifis, A. (2012). Different radiolabelling methods alter the pharmacokinetic and biodistribution properties of Plasminogen Activator Inhibitor Type 2 (PAI-2) forms. *Nuclear Medicine and Biology*, 39 (6), 833-839.

### Authors

Marie Ranson, Paula Berghofer, Kara L. Vine, Ivan Greguric, Rachael Shepherd, and Andrew Katsifis

**Different Radiolabelling Methods Alter the Pharmacokinetic and Biodistribution Properties of Plasminogen Activator Inhibitor Type 2 (PAI-2) Forms**

**Abbreviated title:** Pharmacokinetics and Biodistribution of PAI-2

Marie Ranson<sup>a,b\*</sup>, Paula Berghofer<sup>a,c</sup>, Kara L. Vine<sup>a,b</sup>, Ivan Greguric<sup>a,c</sup>, Rachael Shepherd<sup>c</sup> and Andrew Katsifis<sup>a,c</sup>.

<sup>a</sup>*School of Biological Sciences, University of Wollongong, Wollongong, New South Wales, 2522, Australia*

<sup>b</sup>*Illawarra Health and Medical Research Institute, University of Wollongong, Wollongong, New South Wales, 2522, Australia*

<sup>c</sup>*LifeSciences, Australian Nuclear Science and Technology Organisation, Menai, New South Wales, 2234, Australia*

**Corresponding author:**

Tel: +61 242 3291; fax: +61 242 8130

E-mail address: [mranson@uow.edu.au](mailto:mranson@uow.edu.au)

## **Abstract**

**Introduction:** Tumour-associated urokinase plasminogen activator (uPA) is a critical marker of invasion and metastasis, and it is recognised as having strong prognostic relevance as well as being a therapeutic target. The specific uPA inhibitor plasminogen activator inhibitor type-2 (PAI-2, SerpinB2) specifically targets cell bound uPA and is internalised. Furthermore, preclinical studies have established the “proof-of-principle” of uPA-targeting by PAI-2-cytotoxin conjugates in human carcinoma models. However, these studies also suggest that PAI-2 is rapidly cleared via the renal system with low total dose reaching the tumour. In this study, a comparative single photon emission computed tomography (SPECT) and biodistribution (BD) analysis of different forms of PAI-2 labelled with the radioisotopes iodine-123 ( $^{123}\text{I}$ ) and technetium-99m ( $^{99\text{m}}\text{Tc}$ ) was undertaken.

**Methods:** The pharmacokinetic (PK) properties and BD of wild-type,  $\Delta\text{CD}$ -loop and PEGylated  $\Delta\text{CD}$ -loop PAI-2 labelled with the commonly used diagnostic SPECT radioisotopes  $^{99\text{m}}\text{Tc}$  or  $^{123}\text{I}$  were compared in mouse models of human prostate carcinoma. Whole body SPECT imaging was also performed.

**Results:** Both wild-type or the shorter but active  $\Delta\text{CD}$ -loop form of PAI-2  $^{123}\text{I}$ -labelled indirectly via conjugation to free amine groups (termed  $^{123}\text{I}$ -Bn-PAI-2) exhibited low tumour uptake, rapid excretion and similar PK profiles. Preliminary studies with a short branched-chain PEGylated  $^{123}\text{I}$ -Bn-PAI-2  $\Delta\text{CD}$ -loop indicated an increase in blood retention time and tumour uptake. All  $^{123}\text{I}$ -Bn-labelled radiotracers were largely excreted through the kidneys. By comparison, both wild-type  $^{123}\text{I}$ -PAI-2 (labelled directly via tyrosine residues) and  $^{99\text{m}}\text{Tc}$ -PAI-2 displayed different PK/BD patterns compared to  $^{123}\text{I}$ -Bn-PAI-2, suggesting greater liver based catabolism and thus slower elimination. SPECT imaging mimicked the BD results of all radiotracers.

**Conclusion:** The different labelling methods gave distinct PAI-2 BD and tumour uptake profiles, with radioiodination resulting in the best non-tumour organ clearance profiles. Preliminary analyses with short branched-chain PEGylated  $^{123}\text{I}$ -Bn-PAI-2  $\Delta\text{CD}$ -loop suggest that further investigations with other PEGylation reagents are required to optimise this approach for tumour imaging. These findings impact on the use of PAI-2 for drug delivery and/or diagnostic development.

**Key Words:** Plasminogen activator inhibitor type 2 (PAI-2), serpinB2, small animal SPECT, pharmacokinetics/biodistribution, iodine-123, technetium-99m.

**Abbreviations:** BD, biodistribution; ID/g, injected dose per gram; PEG, polyethylene glycol; PK, pharmacokinetic; PAI-2, plasminogen activator inhibitor type 2; serpin, serine protease inhibitor; uPA, urokinase plasminogen activator;  $\Delta$ CD-loop, loop connecting helices C and D in PAI-2; QTOF-ESI MS, quaternary time of flight electrospray ionisation mass spectrometry; SPECT, Single Photon Emission Computer Tomography.

## 1. Introduction

With an aging population, the worldwide incidence and mortality of cancer is ever increasing and many different methods of diagnosis and therapy have been investigated with varying levels of success [1]. Numerous receptor based targets have been considered for their potential exploitation as targeting entities for use in nuclear medicine. The Urokinase Plasminogen Activation (uPA) system is one such physiological process that is implicated in tumour invasion and metastasis and has the potential for exploitation in this manner, as over-expression of tumour cell surface uPA has strong prognostic relevance as well as being a therapeutic target [2, 3]. uPA is synthesised and secreted as a zymogen whose activation is markedly accelerated upon binding with high affinity to specific cell surface uPA receptors (uPAR). Active, receptor-bound uPA then efficiently converts any cell surface-bound zymogen plasminogen into the highly active, serine protease plasmin, which promotes tissue degradation and remodelling of the local extracellular environment [4]. The specific uPA inhibitor human plasminogen activator inhibitor type-2 (PAI-2, serpinB2) efficiently inhibits uPAR-bound uPA resulting in proteolytic inhibition and rapid and specific receptor-mediated endocytosis of the uPAR/uPA:PAI-2 complex [5-8]. PAI-2 is thus able to efficiently and specifically deliver and concentrate attached cytotoxins within targeted cells [5, 9]. PAI-2 labeled by chelation with the cytotoxic alpha-emitting radionuclide Bismuth-213 ( $^{213}\text{Bi}$ ), targets and significantly reduces tumour growth of human uPA expressing tumours in mouse models [5, 10-12]. Due to the over-expression of uPA in metastatic cells, PAI-2 could possibly be exploited as a highly specific imaging tool for determining the metastatic potential of tumours.

PAI-2 has high stability in plasma, is non-immunogenic and non-toxic, and has been successfully radiolabelled with the isotopes  $^{213}\text{Bi}$  [10, 11, 13] and  $^{125}\text{I}$  [14] which do not interfere with the protein's uPA inhibitory action. Previous biodistribution (BD) studies in human colorectal tumour-bearing mouse models using human recombinant wild-type PAI-2 radioiodinated directly with  $^{125}\text{I}$  via tyrosine residues, shows rapid clearance from all organs of the animal, with a small amount of uptake in the tumour (1.3% injected dose/g) at early time points [14]. Although this excretion profile is ideal for a diagnostic radiotracer, it is important to increase the tumour uptake of PAI-2 while lowering

radioactivity retention in all normal organs in order to optimise imaging potential and/or drug delivery profiles.

Previous studies have shown that the position, type and structure of the radiolabel can greatly influence the organ and tumour uptake and clearance profiles of proteins and peptides [15, 16]. Furthermore, the ultimate application will dictate the radiolabelling approach to use. SPECT is a commonly used imaging modality. The most commonly used radioisotope for SPECT imaging is  $^{99m}\text{Tc}$ , which has a moderately short half-life of 6.02 h and is generally conjugated to proteins or peptides via metal chelators such as diethylenetriamine pentaacetic acid (DTPA) or 1,4,7,10-tetraazacyclododecane- $N,N',N'',N'''$ -tetraacetic acid (DOTA), or via various amino thiols. Both factors may alter the pharmacokinetic (PK) and BD properties of the ligand [17]. The SPECT imaging isotope  $^{123}\text{I}$  has a similar energy profile to  $^{99m}\text{Tc}$  but has potential advantages. For example,  $^{123}\text{I}$  has the highest specific activity available (i.e. has minimal carrier iodine) and can be easily replaced with  $^{124}\text{I}$  for use in PET systems or  $^{131}\text{I}$  for therapy. However, radioiodine attached directly to proteins tends to be unstable *in vivo* with the radiolabelled protein being rapidly dehalogenated resulting in thyroid uptake and excretion of free radioiodine [18]. This can be avoided by indirectly labelling the protein by conjugation of a radioiodinated prosthetic group to free amines [18]. A comparative assessment of these different radiolabelling methods on the PK and BD of PAI-2 has not been previously undertaken.

An alternative approach to modulating PK and BD profiles of imaging and therapeutic protein-based radiopharmaceutical agents is to modify the protein. This is very well exemplified with targeting antibodies and their fragments [19] with small (6.5 kDa) affibody molecules showing promise for improved imaging of HER-2 positive tumours [20]. Structurally, wild-type PAI-2 (47 kDa) consists of three  $\beta$ -sheets, 9  $\alpha$ -helices and a reactive centre loop (that contains the protease recognition site) [21]. PAI-2 also contains a so-called CD-loop, a sequence of 33 amino acids between the C and D  $\alpha$ -helices that may be involved in various intracellular functions [22], but is not required for uPA inhibition [23]. Removal of the CD-loop to generate the shortened form of PAI-2 ( $\Delta$ CD-loop PAI-2; ~44 kDa) is simpler to express and purify recombinantly, retains full uPA inhibitory characteristics [23] and may potentially exhibit a more favourable PK profile

for imaging as is typically seen when the size of a targeting protein is decreased [24]. The circulation of proteins can also be modified by PEGylation, via conjugation of one or more polyethylene glycol (PEG) units [25]. Addition of PEG groups to targeting moieties has the significant effect of increasing the residence time in the blood stream (due to retardation of renal clearance), hence increasing the bioavailability and clinical potency of the drug [25, 26]. This approach has also been used to increase tumour uptake while decreasing kidney uptake of radiolabeled diabodies for improved SPECT imaging purposes [27].

Evaluation of modified forms of PAI-2 using different radiolabelling techniques via PK and BD analyses and SPECT imaging, would allow a direct comparison to the known properties of the PK and BD of wild-type  $^{125}\text{I}$ -PAI-2 [14]. The aim of this study was thus to compare the effect of different  $^{123}\text{I}$  versus  $^{99\text{m}}\text{Tc}$  radiolabelling methods with modified PAI-2 forms on PK and BD profiles, with a further view to optimising tumour uptake of the radiopharmaceutical for the purpose of tumour imaging and/or radiotherapy.



## 2. Materials and Methods

### 2.1 General

Chemicals and solvents were purchased from Sigma-Aldrich unless otherwise indicated. All reagents and solvents were of the highest commercially available grade and used without further purification.  $^{123}\text{I}$  was produced by the National Medical Cyclotron, Sydney, Australia, using the  $^{124}\text{Xe}$  (p, 2n) reaction and was delivered as  $^{123}\text{I-NaI}$  in 0.02 mol/L NaOH at a concentration of 37 GBq/mL.  $^{99\text{m}}\text{Tc}$  obtained from a Gentech® Molybdenum- $^{99}\text{Mo}$ /Technetium generator (ANSTO Health, Lucas Heights, Australia). IsoLink™ was obtained from Mallinckrodt (Covidien). Zeba desalt spin columns were purchased from Quantum Scientific. (Methyl-PEO<sub>12</sub>)-PEO<sub>4</sub>-NHS ester (2420.80 Da) was purchased from Pierce Protein Research Products (Thermo Fisher Scientific, USA). Human recombinant wild-type (47 kDa) and  $\Delta\text{CD-loop}$  (44 KDa) PAI-2 were provided by PAI-2 Pty Ltd (Sydney, Australia) or made in-house as described [23].

### 2.2 Radiolabelling

Radioiodination of both wild-type and  $\Delta\text{CD-loop}$  PAI-2 was performed using direct and indirect methods. Direct radiolabelling was performed using a modified Bolton-Hunter method employing Iodogen (10-50  $\mu\text{g}$ ) as the oxidant together with the protein (5-50  $\mu\text{g}$ ) in PBS (pH 7.4) and  $\text{Na}^{123}\text{I}$  (40-800 MBq). Unincorporated  $^{123}\text{I}$  was separated from protein purified using a Zeba desalt spin column as per manufacturer's instructions. An incorporation yield of  $^{123}\text{I}$  onto PAI-2 of 15-30% was obtained by this method. Quality control and radiochemical stability were ascertained on a radio-analytical HPLC system consisting of a Waters 616 pump, a Waters 486 UV-vis (UV=280 nm) with an inline  $\gamma$  -detector (Ortec) and a Biosep 2000 Phenomenex column (300 x 7.8 mm) or 3000 Phenomenex column (75 x 7.5mm) at 1 ml per min, using a phosphate buffer 100 mM, pH 7.4, NaCl 150 mM mobile phase. The purity and stability of the resultant  $^{123}\text{I}$ -PAI-2 was found to be greater than 95% at room temperature for a minimum of 2 h as assessed by radio-analytical HPLC chromatography. The indirect radiolabelling method was based on a previously described method [28] and involved the conjugation of  $^{123}\text{I-N}$ -succinimidyl 3-iodobenzoate (prepared from the corresponding stannane) to free amine

groups of the PAI-2 protein. Briefly, to *N*-succinimidyl 3-trimethylstannyl benzoate (0.25 mg) in 300  $\mu$ L of acetic acid/methanol 5/95 was added 770 MBq (80  $\mu$ L) of Na<sup>123</sup>I in 0.02 M NaOH and 30  $\mu$ L of Chloramine-T (1 mg /300  $\mu$ L of acetic acid/methanol 5/95). After 5 min at room temperature with shaking, the solution was purified by semi-preparative HPLC as described above (except that a Phenomenex Bondclone C18 column (10  $\mu$ m, 300  $\times$  7.8 mm) was used) to obtain the <sup>123</sup>I-*N*-succinimidyl 3-iodobenzoate in 55-70% incorporation yields. The radiotracer was evaporated to dryness, and then PAI-2 (30 - 60  $\mu$ g in 200  $\mu$ L 0.1 M phosphate buffer, pH 8.5) was added to the activity and shaken for approximately 30 min at room temperature. The mixture was purified using a Zeba desalt spin column as per manufacturer's instructions and the resulting <sup>123</sup>I-3-iodobenzoyl-PAI-2 (<sup>123</sup>I-Bn-PAI-2) in 20-40% radiochemical yield was formulated in PBS pH 7.4 containing 0.01% Tween 80 for use in biological evaluations. The radiotracer was stable (greater than 95%) at room temperature for a minimum of 3 h as measured by radio-analytical HPLC. A representative chromatogram is shown in Supplementary Figure 1.

Radiolabelling of wild-type PAI-2 with <sup>99m</sup>Tc was performed using PAI-2-DTTA [13] using a method modified from Vera et al. [29]. <sup>99m</sup>Tc 100 – 300 MBq and PAI-2-DTTA were added together at a ratio of approximately 1  $\mu$ g protein: 0.55 MBq<sup>99m</sup>Tc in 250  $\mu$ L 0.9% saline and mixed by bubbling nitrogen through the solution for 10 min. Then 250  $\mu$ L of 0.5 mM ascorbic acid in 0.9% saline was added followed immediately by the addition of 25  $\mu$ L of 1 mM acidified tin chloride solution (made fresh by addition of 75  $\mu$ L of HCl (37%) to 5 mg of SnCl<sub>2</sub>, followed by 25  $\mu$ L of 0.9% saline). The reaction was incubated at room temperature in the dark for 50 min and then centrifuged at 2000 *g* for 10 min after which time a one-tenth volume of 10  $\times$  sterile PBS (pH 7.4) was added. The mixture was purified using a Zeba desalt spin column as above and the radiotracer analysed by radio-analytical HPLC also as described above. The percent incorporation was > 95%.

All radiolabelling procedures were performed at least three times. Protein stability and inhibitory activity of the radiolabelled PAI-2 species were confirmed by their ability to form complexes with active uPA as detected by SDS-PAGE and autoradiography as previously described [12-14] (*data not shown*).

### 2.3 PEGylation of PAI-2

PEGylation of PAI-2  $\Delta$ CD-loop was performed by conjugation of the protein with the branched (methyl-PEO<sub>12</sub>)-PEO<sub>4</sub>-NHS ester as described by the manufacturer and adapted from Hermanson [30]. Briefly, 25 mM (methyl-PEO<sub>12</sub>)-PEO<sub>4</sub>-NHS ester freshly dissolved in anhydrous dimethyl formamide was added to 1 mg/mL PAI-2 in phosphate buffer (pH 8.0) to give > 20-fold molar excess of the PEG reagent to protein. The reaction mixture was incubated for at least 3 h at 37°C after which the PEGylated protein was purified away from non-reacted PEGylation reagent using a Zeba desalt spin column as above. Protein conjugation and inhibitory activity was confirmed as described above. In general, >80 % of the protein was PEGylated with 1- 4 PEG groups achieved as determined by SDS-PAGE and QTOF-ESI mass spectrometry (Supplementary Figure 2).

### 2.4 Cell lines and animals

PC-3 human prostate carcinoma cell lines were cultured in RPMI-1640 supplemented with 10% FCS at 37°C under 5% CO<sub>2</sub>: 95% atmosphere and cell surface expression of uPAR and uPA was verified by indirect immunofluorescence using dual colour flow cytometry as previously described [5].

Animal experiments were performed in compliance with the NHMRC Australian Code of Practice for the care and use of animals for scientific purposes and sanctioned by the University of Wollongong and ANSTO Animal Care and Ethics Committees. Male BALB/C nude mice were purchased aged 4-5 weeks old from the Animal Resources Centre (Canning Vale, WA, Australia). Mice were inoculated subcutaneously in the flank with  $1 \times 10^7$  PC-3 human prostate adenocarcinoma cells. All animals were used approximately 3 weeks after inoculation of PC-3 cells at which stage tumours could be palpated in ~90% of mice. Animals used for experiments carried tumours no greater than 12mm and no less than 5mm in diameter. Tumours were positive for uPA expression as determined by immunohistopathological methods (Supplementary Figure 3) as previously described [12].

### 2.5 SPECT Imaging

To further study the pharmacokinetic profiles and hence determine the tumour imaging potential of the above radiotracers, SPECT imaging was performed using a high

resolution  $\gamma$ -camera (X-SPECT<sup>TM</sup>, Gamma Medica Inc, USA), designed for laboratory animals. The  $\gamma$ -camera is equipped with an array of discrete  $2 \times 2 \times 6$  mm NaI(Tl) crystals optically isolated from each other and a high resolution parallel hole collimator with a  $12.5 \times 12.5$  cm field of view. PC-3 tumour bearing mice were anaesthetised via inhalant isoflurane (Forthane<sup>TM</sup>) in 200 mL/min oxygen using a nose cone fitted to the animal bed and planar imaged at 5-30 min, 1, 3, 6 and 24 h after intravenous injection of 7-10 MBq radiotracer. Animal body temperature was maintained with a warm air blower during anesthesia. Prior to imaging, the field of view was corrected for uniformity by filling a Perspex phantom with 80 MBq of <sup>123</sup>I or <sup>99m</sup>Tc and allowing 20,000 counts to be collected. After the uniformity table was collected and applied, the same phantom was rescanned collecting 3000 counts for quality control purposes. QC results indicated the standard deviation in the field of view was < 6% at all times.

## 2.6 Biodistribution (BD)

To quantitatively evaluate the pharmacokinetic properties of the various PAI-2 radiotracers, BD studies were conducted in PC-3 tumour bearing mice. Animals were injected with 0.37 – 0.74 MBq of the various radiotracers in 100  $\mu$ L saline through the lateral tail vein and sacrificed by cervical fracture under the influence of CO<sub>2</sub> between 5 min and 24 h after injection. Blood and selected organs were weighed and their radioactivity measured with a  $\gamma$ -counter (Wallac 1480). The percent of injected activity in each organ was calculated by comparison to suitable dilutions of the total dose of the radiotracer injected. The amount of radioactivity in each organ, expressed in terms of percent of injected dose (% ID) was found by dividing the % ID for each organ by the weight of the organ (% ID/g), corrected for the amount of radioactivity remaining in the tail (always < 9%). Blood clearance profiles were determined by plotting the percentage of the injected dose remaining in the blood over time post radiotracer injection and fitted to a one or two phase exponential decay model using GraphPad Prism version 5.00 for Windows, (GraphPad Software, San Diego CA USA). All values were corrected for radioactivity decay and 5 mice were used for each time point.

## 2.7 *Statistics*

Statistical significance of different groups was determined using two-way ANOVA or paired two-tailed Students T-test (GraphPad Prism V 5.1; San Diego, CA, USA). *P* values < 0.05 were considered statistically significant.

### 3. Results

#### 3.1 SPECT Imaging Studies

The whole body distribution of wild-type  $^{123}\text{I}$ -PAI-2,  $^{123}\text{I}$ -Bn-PAI-2 and  $^{99\text{m}}\text{Tc}$ -PAI-2 in mice bearing human prostate carcinoma was first compared by SPECT imaging over 24 h. Figure 1 shows representative SPECT images acquired at 3 h post radiotracer injection where obvious differences in radiotracer distribution could be seen between all 3 radiolabelling methods. By 3 h, very little radioactivity remained in the kidneys after injection of  $^{123}\text{I}$ -Bn-PAI-2 with the majority of radioactivity detected in the bladder (Figure 1A).  $^{123}\text{I}$ -PAI-2, prepared by the direct radioiodination method, displayed a different biodistribution pattern to that of  $^{123}\text{I}$ -Bn-PAI-2 (Figure 1B) that is suggestive of radiotracer being also taken-up into the liver-hepatobiliary system. As previously reported for other proteins radioiodinated directly via their tyrosine residues [18], the increased radioactivity in the thyroid after injection with  $^{123}\text{I}$ -PAI-2 (Figure 1B) compared to  $^{123}\text{I}$ -Bn-PAI-2 (Figure 1A), suggests significant dehalogenation of  $^{123}\text{I}$ -PAI-2, possibly via *in vivo* metabolism of the protein.  $^{99\text{m}}\text{Tc}$ -PAI-2 resulted in even greater uptake of radioactivity into excretory organs (Figure 1C). Renal excretion within the first 40 min was evident from bladder accumulation of radioactivity following both  $^{123}\text{I}$ -PAI-2 and  $^{99\text{m}}\text{Tc}$ -PAI-2 administration. For all radiotracers very little tumour accumulation was observed.

The imaging patterns of indirectly labelled wild-type PAI-2 ( $^{123}\text{I}$ -Bn-PAI-2) versus the  $\Delta\text{CD}$ -loop form ( $^{123}\text{I}$ -Bn-PAI-2  $\Delta\text{CD}$ -loop) indicated that  $^{123}\text{I}$ -Bn-PAI-2  $\Delta\text{CD}$ -loop was perhaps even more rapidly cleared via renal excretion as the only remaining radioactivity that could be detected by 3 h was in the bladder (Figure 1D). SPECT images of mice acquired within 5 to 20 min after either radiotracer injection indicated that radioactivity was rapidly disseminated throughout the body, with accumulation in the bladder evident within 5 – 10 min, especially for the CD-loop form (*data not shown*). PEGylated  $^{123}\text{I}$ -Bn-PAI-2  $\Delta\text{CD}$ -loop followed a similar imaging pattern to non-PEGylated  $^{123}\text{I}$ -Bn-PAI-2  $\Delta\text{CD}$ -loop though the level of circulating radioactivity at 3 h post injection (Figure 1E) appeared to be higher than for the non-PEGylated radiotracer (Figure 1D).

These observations were confirmed quantitatively as described in the following PK and BD studies.

### 3.2 Blood clearance evaluations

As suggested by SPECT imaging, blood levels of radioactivity in mice injected with  $^{123}\text{I}$ -Bn-PAI-2 or  $^{123}\text{I}$ -Bn-PAI-2  $\Delta\text{CD}$ -loop rapidly declined between 5 and 60 min (Figure 2A and B, respectively). This was especially the case for  $^{123}\text{I}$ -Bn-PAI-2  $\Delta\text{CD}$ -loop, with radioactivity reaching detection limits 3 h after administration (Figure 2B). There was no distinction between distribution and elimination phases of the radioactivity as the data best fit a one-phase decay model for both radiotracers with half lives of approximately 17 and 12 min for the wild-type and  $\Delta\text{CD}$ -loop PAI-2 forms, respectively. These values corresponded to the SPECT images where radioactivity was rapidly eliminated via the kidneys with minimal metabolism as evidenced by no accumulation of  $^{123}\text{I}$  in the thyroid for either  $^{123}\text{I}$ -Bn-PAI-2 or  $^{123}\text{I}$ -Bn-PAI-2  $\Delta\text{CD}$ -loop. In contrast, directly radioiodinated wild-type PAI-2 exhibits a biphasic PK profile [14] and was seen by SPECT (refer to Figure 1B) to reside in the body for longer than the indirectly labelled forms (refer to Figures 1A and D). However, PEGylated  $^{123}\text{I}$ -Bn-PAI-2  $\Delta\text{CD}$ -loop also exhibited a biphasic pharmacokinetic profile consisting of an initial decay phase of rapid radioactivity distribution ( $\sim 7$  min) followed by a low decay phase of radioactivity clearance ( $\sim 111$  min) (Figure 2C). Compared to the non-PEGylated species there was increased blood retention of radioactivity by 3 h after administration, which was also somewhat reflected in the blood distribution seen in the SPECT images (refer to Figure 1E).

The  $^{99\text{m}}\text{Tc}$ -PAI-2 (wild-type) data best fits a one-phase decay model. Significant amounts of radioactivity remained in the blood 24 h after injection as reflected by a longer  $T_{1/2}$  of 90 min (Figure 2D). This also compared well to the SPECT images (refer to Figure 1C) suggestive of a longer residence time of  $^{99\text{m}}\text{Tc}$ -PAI-2 in mice compared to any of the radioiodinated protein forms.

### 3.3 Biodistribution

The BD patterns of the differently radiolabelled PAI-2 forms in mice bearing prostate tumours were determined over 24 h. Within the first 30 min after injection of  $^{123}\text{I}$ -Bn-PAI-2  $\Delta\text{CD}$  loop, kidneys and livers exhibited the greatest uptake of radioactivity which quickly declined thereafter (Table 1). This pattern was reflected in the other organs analysed with any substantial uptake ( $> 2\%$  ID/g), except for thyroid and tumour (discussed further below). Whilst a similar metabolic pattern for most organs was seen after administration of  $^{123}\text{I}$ -Bn-PAI-2, kidney uptake and elimination of radioactivity levels was slower than for  $^{123}\text{I}$ -Bn-PAI-2  $\Delta\text{CD}$ -loop in the first hour (Table 1). After 1 h, very little ( $<6\%$  or  $< 1\%$  for wild-type versus  $\Delta\text{CD}$ -loop forms, respectively) of the total injected dose/g of the radioiodinated proteins remained in any organ indicating very fast elimination, as suggested by the blood clearance patterns, especially for PAI-2  $\Delta\text{CD}$ -loop. PEGylation did not substantially alter the BD patterns of  $^{123}\text{I}$ -Bn-PAI-2  $\Delta\text{CD}$ -loop for most organs except for the liver and kidneys, where uptake of radioactivity was significantly lower at 5 – 30 min and 30 min post injection ( $p < 0.05$ ), respectively, compared to non-PEGylated  $^{123}\text{I}$ -Bn-PAI-2  $\Delta\text{CD}$ -loop (Table 1). The metabolic pattern of  $^{99\text{m}}\text{Tc}$ -PAI-2 differed from all of the radioiodinated forms where substantial uptake of radioactivity was evident within the first 5 min after injection into all major organs including heart and lungs, with very slow to no clearance seen after 6 h (Table 1). Indeed, after 24 h many organs still retained  $> 4\%$  ID/g.

The thyroid uptake of radioactivity after either  $^{123}\text{I}$ -Bn-PAI-2,  $^{123}\text{I}$ -Bn-PAI-2  $\Delta\text{CD}$ -loop or PEGylated  $^{123}\text{I}$ -Bn-PAI-2  $\Delta\text{CD}$ -loop injection was low with minimal difference in levels over time between radiotracers (Table 1). While  $^{99\text{m}}\text{Tc}$ -PAI-2 showed higher thyroid uptake overall, these values were still relatively low (minimal thyroid uptake seen in SPECT images shown in Figure 1).

The pattern of tumour uptake of radioactivity was somewhat modulated by the different radiolabelling methods and modifications to PAI-2 protein (Figure 3). For the wild-type protein, radioiodination versus radiometal labelling resulted in significantly different radioactivity uptake levels at all time points ( $p < 0.01$ ) (Figure 3A). A maximum uptake of  $0.85 \pm 0.24\%$  ID/g occurred at 60 min after  $^{123}\text{I}$ -Bn-PAI-2 injection with a steady decline in radioactivity levels thereafter. In contrast, radioactivity levels peaked at



1.63 ± 0.33 %ID/g at 5 min after <sup>99m</sup>Tc-PAI-2 injection and were retained at this level for 3 h (Figure 3A) before decreasing substantially (*data not shown*). A comparison of the indirectly radioiodinated wild-type versus ΔCD-loop PAI-2 forms found no significant differences in tumour uptake of radioactivity following injection of either radiotracer at any time points (Figure 3B). However, in contrast to <sup>123</sup>I-Bn-PAI-2, tumour uptake of radioactivity peaked at 30 min (0.88 ± 0.12 %ID/g) post <sup>123</sup>I-Bn-PAI-2 ΔCD-loop injection (Figure 3B). For both radiotracers, tumour radioactivity levels declined to < 0.2 % ID/g by 3 h after injection (Figure 3B). PEGylated <sup>123</sup>I-Bn-PAI-2 ΔCD-loop resulted in a maximum uptake of radioactivity at 5 min post injection at a level (1.6 ± 0.22% ID/g) that was significantly greater than that attributable to non-PEGylated <sup>123</sup>I-Bn-PAI-2 ΔCD-loop at this time point (0.71 ± 0.16% ID/g) (p < 0.001) (Figure 3C). Thereafter, the levels of radioactivity in tumours after injection of PEGylated <sup>123</sup>I-Bn-PAI-2 ΔCD-loop compared to non-PEGylated <sup>123</sup>I-Bn-PAI-2 ΔCD-loop were not significantly different from each other (Figure 3C).

#### 4. Discussion

The aim of these studies were to perform a comparative SPECT and BD analysis of radioiodinated versus  $^{99m}\text{Tc}$ -labelled wild-type PAI-2, and radioiodinated wild-type versus the shortened PAI-2  $\Delta\text{CD}$ -loop form in order to assess organ distribution and clearance patterns for potential future development as imaging agents for cancer and for therapeutic radioisotope delivery. Further to this latter application, PEGylation of PAI-2  $\Delta\text{CD}$ -loop was explored as part of an initial investigation to assess the potential to increase tumour uptake for radiotherapy. As expected, the different labelling methods modulated the PK and BD properties of PAI-2 to varying degrees. While no significant benefit in terms of tumour uptake was obtained through use of the shortened version of the protein, PAI-2  $\Delta\text{CD}$ -loop retains full uPA inhibitory activity and is more easily expressed and purified compared to wild-type PAI-2 [23], thus lending itself to a simpler manufacturing process. Moreover PAI-2  $\Delta\text{CD}$ -loop can be modified by PEGylation whilst retaining its activity and prolonging blood retention and tumour uptake of radiotracer.

Compared to directly radioiodinated PAI-2 where radioactivity associated with the thyroid is significant (refer to Figure 1B) due to either dehalogenation and/or metabolism of the radiotracer (intact radioiodinated species were found in plasma 2 h after administration [14]), the very low  $^{123}\text{I}$  levels associated with the thyroid after administration of indirectly radioiodinated wild-type or  $\Delta\text{CD}$ -loop PAI-2 suggest that the radiotracers were not metabolised but rather were cleared via the renal system intact. Whether this is indeed the case would need to be verified by analyses of plasma and urine samples however, the single phase blood clearance properties and minimal uptake by discrete organs other than the kidneys lends favour to this hypothesis. Studies have shown that  $^{111}\text{In}$ -protein complexes achieved using the chelator DOTA may be more stable *in vivo* and result in enhanced tissue accumulation of radioactivity [31]. Indeed this appeared to be the case when comparing organ BD of wild-type  $^{99m}\text{Tc}$ -PAI-2 versus  $^{123}\text{I}$ -Bn-PAI-2 (or  $^{123}\text{I}$ -Bn-PAI-2  $\Delta\text{CD}$ -loop), especially from 30 min onwards after injection. While tumour uptake of radioactivity was also increased and cleared more slowly by

using  $^{99m}\text{Tc}$ -PAI-2 compared to the radioiodinated forms, this is potentially at the detriment of also accumulating radioactivity in non-target organs.

Over the first 3 h in which radioactivity was detectable in tumours by BD studies, tumour uptake using all forms of radiolabelled PAI-2 was many times less than that in the blood on a per gram basis, resulting in no tumour imaging capability. The contrast required to detect tumour masses via imaging compared to normal tissue requires in the least that the amount of radiotracer circulating in blood to be lower than that in the tumour on a percent per gram of tissue basis. However the amount of radiotracer distributed to other non-tumour tissues other than the liver and kidneys, were exceptionally low, particularly after 1 h post radiotracer injection, suggesting potential for further optimisation as a tumour imaging agent.

Directly radioiodinated wild-type  $^{125}\text{I}$ -PAI-2 levels peaked in tumours at 30 - 60 min at 1 – 2 %ID/g [14]. That protein reached the tumours was verified by immunoprecipitation of PAI-2 in previous studies [14]. A similar temporal profile was observed using either  $^{123}\text{I}$ -Bn-PAI-2 (or  $^{123}\text{I}$ -Bn-PAI-2  $\Delta\text{CD}$ -loop), however at no time point did the tumour uptake exceed 1% per gram of tissue. Due to low levels of tumour accumulation, use of radioiodinated PAI-2 as SPECT imaging agents would require further optimisation. A possible explanation for the low tumour uptake of radiotracers is the very short blood half-life of the proteins, as described above, that did not allow distribution of radiotracer to organs and rather were immediately excreted via the kidneys. However, even the small increase in molecular weight obtained through PEGylation of PAI-2  $\Delta\text{CD}$ -loop using the 2420.80 Da branched chain PEG, resulted in biphasic blood clearance patterns compared to the single phase exhibited by the non-PEGylated form (refer to Figure 2), and somewhat increased both retention of the radiotracer in the blood and tumour uptake. These promising preliminary PEGylation studies suggest that further refinement in this area may be obtained to produce better PK properties of the radiotracer for use in radiotherapy. As the PEGylated PAI-2  $\Delta\text{CD}$ -loop form used in this study was less than 70 kDa (Supplementary Figure 2), it is still considered small enough to be eliminated via the renal system [25]. Attachment of longer chain length PEG groups will increase the molecular weight of the PEGylated protein complex [25], and hypothetically lead to longer blood retention thus greater opportunity for PAI-2 to interact with cell surface

associated uPA. Larger PEGylated PAI-2 species would find further application in radiotherapy as the modified protein may increase the payload of conjugated therapeutic radiometals delivered to the tumour whilst decreasing kidney uptake. Success has already been derived using  $^{213}\text{Bi}$ -PAI-2 in targeted alpha particle radiotherapy towards metastatic cancer [11, 12]. We are currently optimizing methods for site-directed conjugation of larger PEG groups using different PEGylation techniques, chain lengths and molecular weights (up to 30 kDa), in order to identify the most advantageous changes in biopharmacokinetic properties to PAI-2.

The human prostate carcinoma mouse model was selected on the basis that the PC-3 cells were, before implantation, shown to express uPA and the model has been used successfully previously for tumour efficacy studies investigating  $^{213}\text{Bi}$ -PAI-2 as a radiopharmaceutical [11]. However, histopathology analysis of the post mortem tumour tissues from BD studies indicated that the pattern of uPA expression in these tumours was somewhat heterogeneous and not widespread (Supplementary Figure 3), which would limit the PAI-2 uptake possibly explaining low tumour radiotracer accumulation. While haematoxylin and eosin staining of the PC-3 tumours showed no necrosis and evidence of angiogenesis, better *in vivo* metastases models in terms of uPA levels should also be investigated. For example, glioma tumour models have been shown to have high uPAR expression [32]. Indeed, using uPAR binding synthetic peptides and the  $^{64}\text{Cu}$  radiolabel, Li *et al.* [32] reported accumulation of up to 8.1 %ID/g of tissue in gliomas at 6 h post injection based on PET imaging studies. Given the potential for the improved imaging properties of peptides compared to larger proteins, the use of PAI-2 mimetics that retain their uPA activity are being investigated. The use of  $^{64}\text{Cu}$ ,  $^{68}\text{Ga}$  or other radioisotopes as a radiolabel for PAI-2 in PET imaging may also be an avenue for exploration.

### **Acknowledgements**

This research was supported in part by AINSE grant 06P150, and a Cancer Institute Fellowship to MR. The authors would like to thank Emma Millard, Kerynne Belbin and Mitchell Quinlivan for involvement in the animal experiments.

## References

- [1] Minchinton AI and Tannock IF. Drug penetration in solid tumours. *Nat Rev Cancer* 2006;6:583-92.
- [2] Croucher DR, Saunders DN, Lobov S, and Ranson M. Revisiting the biological roles of PAI2 (SERPINB2) in cancer. *Nat Rev Cancer* 2008;8:535-45.
- [3] Harris L, Fritsche H, Mennel R, Norton L, Ravdin P, Taube S, et al. American Society of Clinical Oncology 2007 update of recommendations for the use of tumor markers in breast cancer. *J Clin Oncol* 2007;25:5287-312.
- [4] Ranson M and Andronicos NM. Plasminogen binding and cancer: promises and pitfalls. *Front Biosci* 2003;8:s294-304.
- [5] Al-Ejeh F, Croucher D, and Ranson M. Kinetic analysis of plasminogen activator inhibitor type-2: urokinase complex formation and subsequent internalisation by carcinoma cell lines. *Exp Cell Res* 2004;297:259-71.
- [6] Cochran BJ, Croucher DR, Lobov S, Saunders DN, and Ranson M. Dependence on Endocytic Receptor Binding via a Minimal Binding Motif Underlies the Differential Prognostic Profiles of SerpinE1 and SerpinB2 in Cancer. *J Biol Chem* 2011;286:24467-75.
- [7] Croucher D, Saunders DN, and Ranson M. The urokinase/PAI-2 complex: a new high affinity ligand for the endocytosis receptor low density lipoprotein receptor-related protein. *J Biol Chem* 2006;281:10206-13.
- [8] Croucher DR, Saunders DN, Stillfried GE, and Ranson M. A structural basis for differential cell signalling by PAI-1 and PAI-2 in breast cancer cells. *Biochem J* 2007;408:203-10.
- [9] Vine KL, Locke JM, Bremner JB, Pyne SG, and Ranson M. Selective targeting of 2'-deoxy-5-fluorouridine to urokinase positive malignant cells in vitro. *Bioorg Med Chem Lett* 2010;20:2908-11.
- [10] Allen BJ, Tian Z, Rizvi SM, Li Y, and Ranson M. Preclinical studies of targeted alpha therapy for breast cancer using <sup>213</sup>Bi-labelled-plasminogen activator inhibitor type 2. *Br J Cancer* 2003;88:944-50.
- [11] Li Y, Rizvi SM, Ranson M, and Allen BJ. <sup>213</sup>Bi-PAI2 conjugate selectively induces apoptosis in PC3 metastatic prostate cancer cell line and shows anti-cancer activity in a xenograft animal model. *Br J Cancer* 2002;86:1197-203.
- [12] Stutchbury TK, Al-Ejeh F, Stillfried GE, Croucher DR, Andrews J, Irving D, et al. Preclinical evaluation of <sup>213</sup>Bi-labeled plasminogen activator inhibitor type 2 in an orthotopic murine xenogenic model of human breast carcinoma. *Mol Cancer Ther* 2007;6:203-12.
- [13] Ranson M, Tian Z, Andronicos NM, Rizvi S, and Allen BJ. In vitro cytotoxicity of bismuth-213 (<sup>213</sup>Bi)-labeled-plasminogen activator inhibitor type 2 (alpha-PAI-2) on human breast cancer cells. *Breast Cancer Research and Treatment* 2002;71:149-59.
- [14] Hang MTN, Ranson M, Saunders DN, Liang XM, Bunn CL, and Baker MS. Pharmacokinetics and biodistribution of recombinant human plasminogen activator inhibitor type 2 (PAI-2) in control and tumour xenograft-bearing mice. *Fibrinol Proteol* 1998;12:145-54.

- [15] Sharkey RM, Rossi EA, Chang CH, and Goldenberg DM. Improved cancer therapy and molecular imaging with multivalent, multispecific antibodies. *Cancer Biother Radiopharm* 2010;25:1-12.
- [16] Rusckowski M, Qu T, Gupta S, Ley A, and Hnatowich DJ. A Comparison in Monkeys of <sup>99m</sup>Tc Labeled to a Peptide by 4 Methods. *J Nuc Medicine* 2001;42:1870-7.
- [17] Al-Ejeh F, Darby JM, Thierry B, and Brown MP. A simplified suite of methods to evaluate chelator conjugation of antibodies: effects on hydrodynamic radius and biodistribution. *Nucl Med Biol* 2009;36:395-402.
- [18] Vallabhajosula S. Radiopharmaceuticals in Oncology. In: I Khalkhali, JC Maublant, and SJ Goldsmith editors. *Nuclear Oncology: Diagnosis and Therapy*. Philadelphia: Lippincott Williams and Williams; 2001, p. 31-62.
- [19] Kenanova V and Wu AM. Tailoring antibodies for radionuclide delivery. *Expert Opin Drug Deliv* 2006;3:53-70.
- [20] Tolmachev V, Feldwisch J, Lindborg M, Baastrup B, Sandstrom M, and Orlova A. Influence of an aliphatic linker between DOTA and synthetic Z(HER2:342) Affibody molecule on targeting properties of the (<sup>111</sup>In)-labeled conjugate. *Nucl Med Biol* 2011;38:697-706.
- [21] Jankova L, Harrop SJ, Saunders DN, Andrews JL, Bertram KC, Gould AR, et al. Crystal structure of the complex of plasminogen activator inhibitor 2 with a peptide mimicking the reactive center loop. *J Biol Chem* 2001;276:43374-82.
- [22] Lee JA, Cochran BJ, Lobov S, and Ranson M. Forty Years Later and the Role of Plasminogen Activator Inhibitor Type 2/SERPINB2 Is Still an Enigma. *Semin Thromb Hemost* 2011;37:395-407.
- [23] Cochran BJ, Gunawardhana LP, Vine KL, Lee JA, Lobov S, and Ranson M. The CD-loop of PAI-2 (SERPINB2) is redundant in the targeting, inhibition and clearance of cell surface uPA activity. *BMC Biotechnol* 2009;9:43.
- [24] Kim EE. Radioimmunodetection of Cancer. In: EE Kim and DJ Yang editors. *Targeted Molecular Imaging in Oncology* New York: Springer-Verlag; 2001, p. 88-101.
- [25] Veronese FM and Mero A. The impact of PEGylation on biological therapies. *BioDrugs* 2008;22:315-29.
- [26] Pasut G, Sergi M, and Veronese FM. Anti-cancer PEG-enzymes: 30 years old, but still a current approach. *Adv Drug Deliv Rev* 2008;60:69-78.
- [27] Li L, Crow D, Turatti F, Bading JR, Anderson A-L, Poku E, et al. Site-Specific Conjugation of Monodispersed DOTA-PEG<sub>n</sub> to a Thiolated Diabody Reveals the Effect of Increasing PEG Size on Kidney Clearance and Tumor Uptake with Improved <sup>64</sup>Copper PET Imaging. *Bioconjugate Chemistry* 2011;22:709-16.
- [28] Carroll MA and Yan R. Formation of <sup>18</sup>F and <sup>19</sup>F Fluoroarenes Bearing Reactive Functionalities. US 2009/0286992 A1, 2009
- [29] Vera DR, Wallace AM, Hoh CK, and Mattrey RF. A synthetic macromolecule for sentinel node detection: (<sup>99m</sup>Tc)-DTPA-mannosyl-dextran. *J Nucl Med* 2001;42:951-9.
- [30] Hermanson GT. *Bioconjugate Techniques*. Academic Press, Inc; 1996, p. 606-28.
- [31] Kenanova V, Olafsen T, Williams LE, Ruel NH, Longmate J, Yazaki PJ, et al. Radioiodinated versus radiometal-labeled anti-carcinoembryonic antigen single-chain Fv-Fc antibody fragments: optimal pharmacokinetics for therapy. *Cancer Res* 2007;67:718-26.

[32] Li ZB, Niu G, Wang H, He L, Yang L, Ploug M, et al. Imaging of urokinase-type plasminogen activator receptor expression using a  $^{64}\text{Cu}$ -labeled linear peptide antagonist by microPET. *Clin Cancer Res* 2008;14:4758-66.

## Figure Captions

**Figure 1.** Static SPECT planar images obtained 3 h post injection of 10 MBq of each radiotracer as indicated in mice bearing human prostate carcinoma xenografts. Each frame represents an image acquisition time of 5 min. Tumour position is to the right of the bladder (arrow). The scale indicates the highest value in counts/pixel in the image.

**Figure 2.** Blood clearance profiles for (A)  $^{123}\text{I}$ -Bn-PAI-2 (wild-type) (B),  $^{123}\text{I}$ -Bn-PAI-2  $\Delta\text{CD}$ -loop, (C) PEGylated  $^{123}\text{I}$ -Bn-PAI-2  $\Delta\text{CD}$ -loop, and (D)  $^{99\text{m}}\text{Tc}$ -PAI-2 (wild-type) in mice bearing human prostate carcinoma xenografts. The  $T_{1/2}$  values were calculated using non-linear regression and best fitted a one-phase (A, B, and D) and two-phase (C) exponential decay model. Values shown are the means of % ID/g of tissue corrected for tail vein  $\pm$  SD ( $n = 5$ ) (% ID remaining in tail < 10%), from a representative experiment.

**Figure 3.** A comparison of tumour uptake over time for (A) wild-type  $^{123}\text{I}$ -Bn-PAI-2 (●) versus  $^{99\text{m}}\text{Tc}$ -PAI-2 (■), (B) wild-type  $^{123}\text{I}$ -Bn-PAI-2 (●) versus  $^{123}\text{I}$ -Bn-PAI-2  $\Delta\text{CD}$ -loop (▲), and (C)  $^{123}\text{I}$ -Bn-PAI-2  $\Delta\text{CD}$ -loop (▲) versus PEGylated  $^{123}\text{I}$ -Bn-PAI-2  $\Delta\text{CD}$ -loop (◆) in mice bearing human prostate carcinoma xenografts. Values shown are the means of % ID/g of tissue corrected for tail vein  $\pm$  SD ( $n = 5$ ). All curves were compared using two-way ANOVA with Bonferroni post-test.



**TABLE 1.**

Biodistribution of radioiodinated PAI-2 forms and wild-type  $^{99m}\text{Tc}$ -PAI-2 in mice bearing PC-3 prostate carcinoma xenografts. Values are expressed as percent of injected dose per gram (%ID/g) of tissue (mean  $\pm$  SD).

PAI-2 form	Time (min)	Blood	Liver	Kidney	Spleen	Lungs	Heart	Thyroid	Bone
$^{123}\text{I}$ -Bn-PAI-2 (wild-type)*	5	20.39 $\pm$ 3.22	9.78 $\pm$ 1.23	17.11 $\pm$ 3.10	4.69 $\pm$ 0.50	8.45 $\pm$ 1.98	3.871 $\pm$ 0.58	3.35 $\pm$ 0.63	1.71 $\pm$ 0.21
	30	6.13 $\pm$ 0.98	4.89 $\pm$ 0.47	22.31 $\pm$ 2.24	2.68 $\pm$ 0.86	3.17 $\pm$ 0.69	1.88 $\pm$ 0.34	2.85 $\pm$ 0.55	1.04 $\pm$ 0.27
	60	5.05 $\pm$ 0.94	3.41 $\pm$ 0.71	21.65 $\pm$ 3.34	3.00 $\pm$ 2.36	3.25 $\pm$ 0.39	4.16 $\pm$ 5.43	4.18 $\pm$ 3.47	1.48 $\pm$ 0.68
	180	1.25 $\pm$ 0.34	1.03 $\pm$ 0.33	5.57 $\pm$ 0.99	0.59 $\pm$ 0.24	0.80 $\pm$ 0.22	0.41 $\pm$ 0.12	2.73 $\pm$ 1.48	0.30 $\pm$ 0.08
	360	0.44 $\pm$ 0.11	0.35 $\pm$ 0.18	1.41 $\pm$ 0.59	0.55 $\pm$ 0.68	0.39 $\pm$ 0.04	0.15 $\pm$ 0.03	5.86 $\pm$ 4.83	0.29 $\pm$ 0.23
$^{99m}\text{Tc}$ -PAI-2 (wild-type)	5	13.98 $\pm$ 3.22	14.48 $\pm$ 0.01	12.51 $\pm$ 0.82	10.90 $\pm$ 2.11	11.25 $\pm$ 0.85	4.80 $\pm$ 0.26	5.14 $\pm$ 1.03	5.01 $\pm$ 0.69
	30	7.80 $\pm$ 1.44	10.68 $\pm$ 2.11	12.66 $\pm$ 1.39	7.88 $\pm$ 1.98	6.59 $\pm$ 1.09	3.16 $\pm$ 0.54	6.24 $\pm$ 1.49	6.31 $\pm$ 0.68
	60	8.61 $\pm$ 0.65	13.84 $\pm$ 2.19	14.24 $\pm$ 1.54	8.92 $\pm$ 1.72	6.34 $\pm$ 0.61	3.06 $\pm$ 0.23	6.62 $\pm$ 1.38	7.93 $\pm$ 1.34
	180	6.55 $\pm$ 0.72	13.85 $\pm$ 2.52	13.70 $\pm$ 1.61	7.91 $\pm$ 1.24	4.68 $\pm$ 0.38	2.17 $\pm$ 0.31	11.60 $\pm$ 9.62	7.91 $\pm$ 1.26
	360	4.49 $\pm$ 0.44	11.05 $\pm$ 1.69	9.44 $\pm$ 0.55	6.37 $\pm$ 1.96	3.51 $\pm$ 0.49	1.43 $\pm$ 0.27	6.27 $\pm$ 2.00	7.20 $\pm$ 0.89
	1440	2.30 $\pm$ 0.29	5.25 $\pm$ 0.32	4.56 $\pm$ 0.29	4.92 $\pm$ 0.76	1.76 $\pm$ 0.38	0.76 $\pm$ 0.07	4.04 $\pm$ 1.12	7.01 $\pm$ 0.83
$^{123}\text{I}$ -Bn-PAI-2 $\Delta$ CD-loop*	5	17.28 $\pm$ 1.48	15.49 $\pm$ 2.53	33.38 $\pm$ 2.46	5.35 $\pm$ 0.39	8.52 $\pm$ 1.16	3.32 $\pm$ 0.21	2.87 $\pm$ 0.90	1.72 $\pm$ 0.28
	30	4.06 $\pm$ 0.45	8.96 $\pm$ 1.08	34.61 $\pm$ 5.39	4.23 $\pm$ 0.71	4.05 $\pm$ 0.71	1.54 $\pm$ 0.21	3.02 $\pm$ 1.51	1.16 $\pm$ 0.17
	60	1.00 $\pm$ 0.15	2.33 $\pm$ 0.31	7.72 $\pm$ 1.20	1.67 $\pm$ 0.27	1.66 $\pm$ 0.35	0.41 $\pm$ 0.07	1.11 $\pm$ 0.60	0.50 $\pm$ 0.09
	180	0.17 $\pm$ 0.05	0.46 $\pm$ 0.05	0.69 $\pm$ 0.20	0.60 $\pm$ 0.12	0.45 $\pm$ 0.15	0.08 $\pm$ 0.06	2.86 $\pm$ 0.38	0.11 $\pm$ 0.03
	360	0.16 $\pm$ 0.01	0.41 $\pm$ 0.11	0.74 $\pm$ 0.17	0.43 $\pm$ 0.23	0.22 $\pm$ 0.08	0.07 $\pm$ 0.01	5.70 $\pm$ 2.03	0.1 $\pm$ 0.03
PEG $^{123}\text{I}$ -Bn-PAI-2 $\Delta$ CD-loop*	5	15.99 $\pm$ 1.61	7.7 $\pm$ 1.09	32.01 $\pm$ 8.98	3.53 $\pm$ 0.35	7.14 $\pm$ 1.11	3.88 $\pm$ 1.09	4.76 $\pm$ 1.47	2.00 $\pm$ 0.59
	30	5.67 $\pm$ 0.55	3.33 $\pm$ 0.53	11.93 $\pm$ 1.15	1.98 $\pm$ 0.12	3.58 $\pm$ 0.54	1.87 $\pm$ 0.36	6.20 $\pm$ 2.03	2.11 $\pm$ 1.53
	60	4.51 $\pm$ 0.25	1.95 $\pm$ 0.16	8.47 $\pm$ 0.83	1.48 $\pm$ 0.08	2.51 $\pm$ 0.34	1.47 $\pm$ 0.16	4.79 $\pm$ 1.48	0.74 $\pm$ 0.17
	180	1.81 $\pm$ 0.14	0.76 $\pm$ 0.08	2.32 $\pm$ 0.43	0.68 $\pm$ 0.05	1.32 $\pm$ 0.41	0.58 $\pm$ 0.08	0.58 $\pm$ 0.08	0.31 $\pm$ 0.03
	360	1.25 $\pm$ 0.30	0.50 $\pm$ 0.22	1.28 $\pm$ 0.54	0.94 $\pm$ 1.02	0.77 $\pm$ 0.27	0.41 $\pm$ 0.14	0.41 $\pm$ 0.14	0.21 $\pm$ 0.09

Data are corrected for tail vein (% ID remaining in tail < 10%), n = 5.

Muscle contained <1.5% per gram and brain contained <0.6% per gram at all time points for all radiotracers

\* Data not shown for 1440 min (24 h) as all values <0.12% except for thyroid.

Figure 1

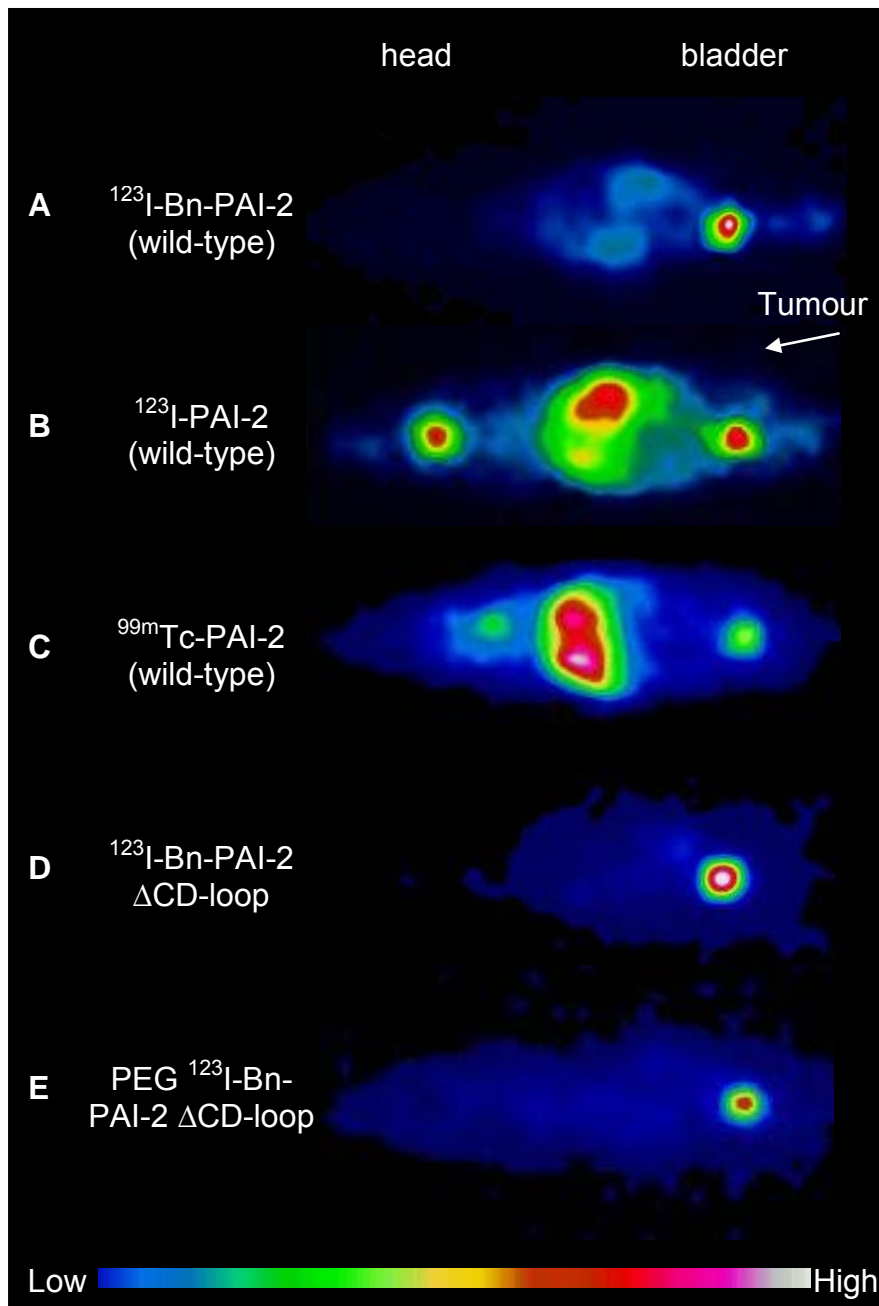
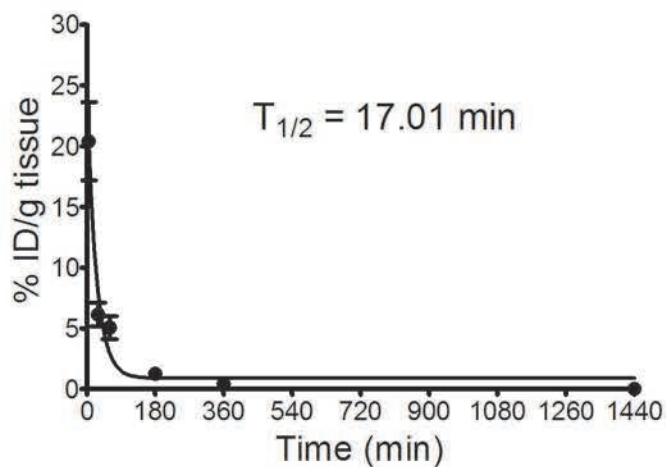
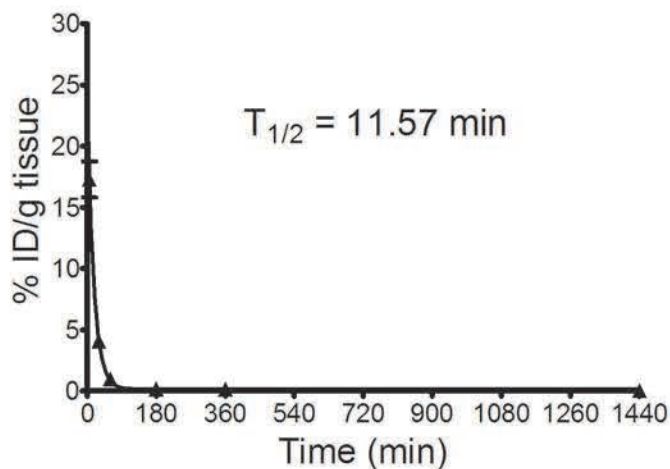


Figure 2

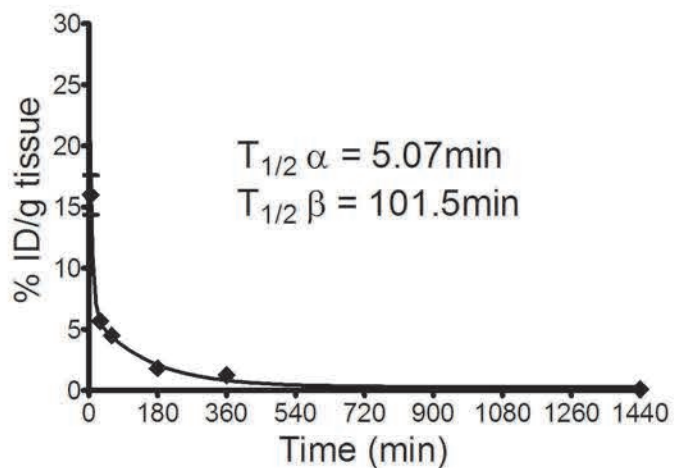
A.  $^{123}\text{I}$ -Bn-PAI-2



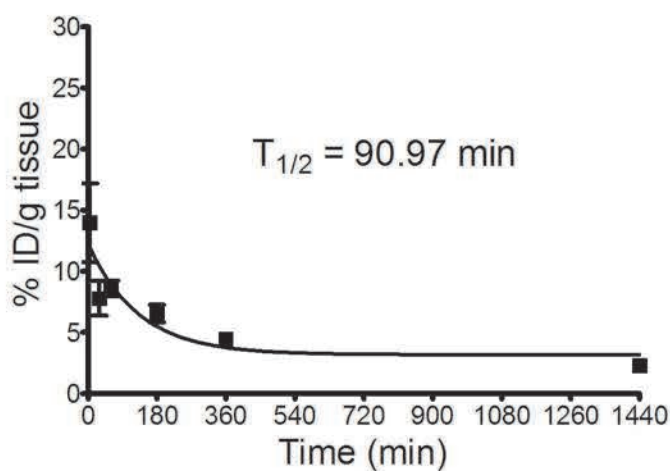
B.  $^{123}\text{I}$ -Bn-PAI-2  $\Delta$ CD-loop



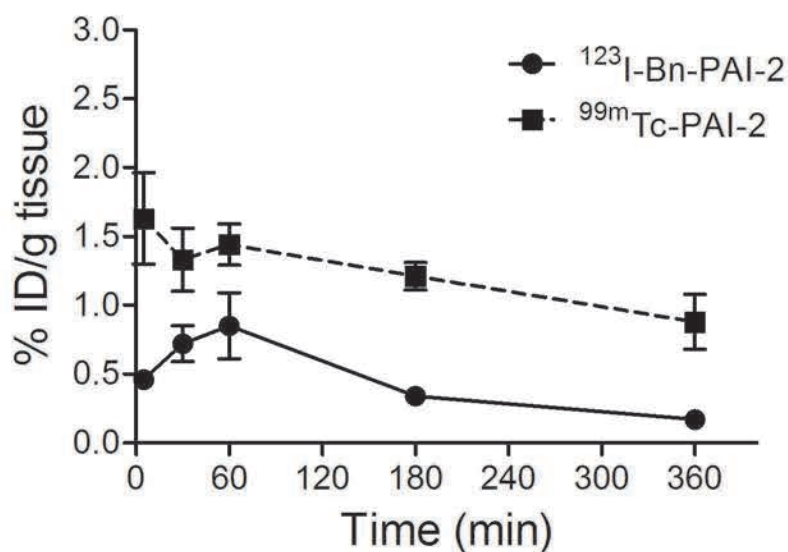
C. PEG  $^{123}\text{I}$ -Bn-PAI-2  $\Delta$ CD-loop



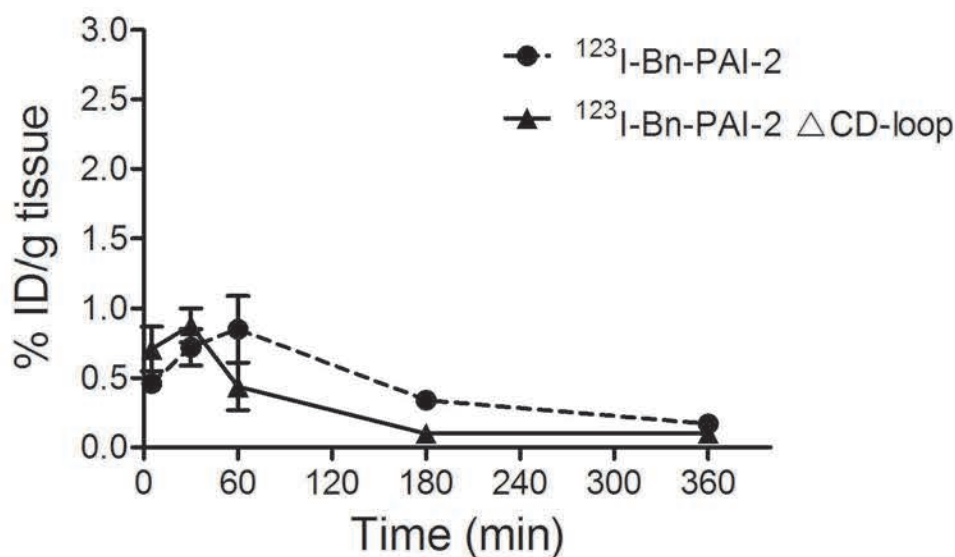
D.  $^{99\text{m}}\text{Tc}$ -PAI-2



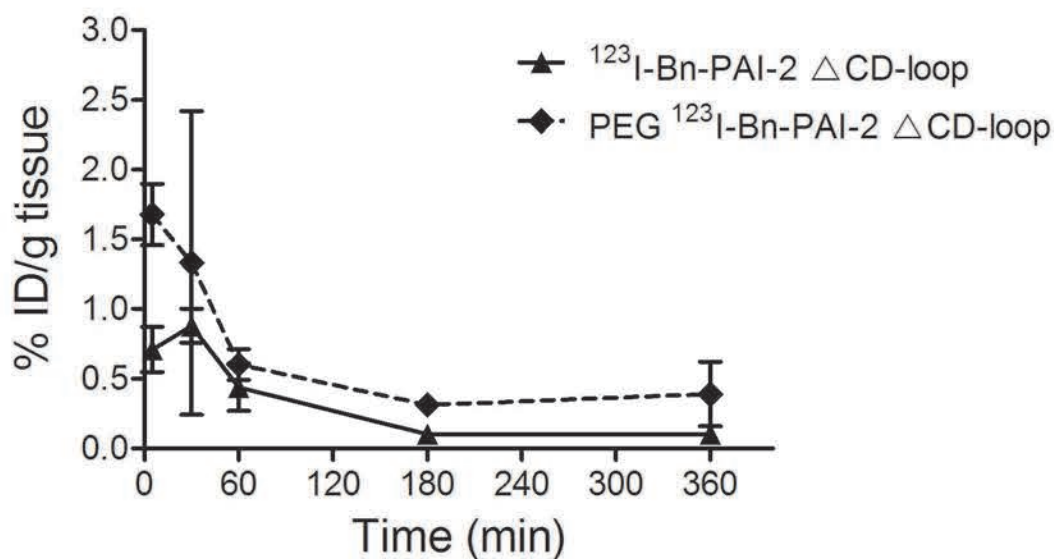
A.



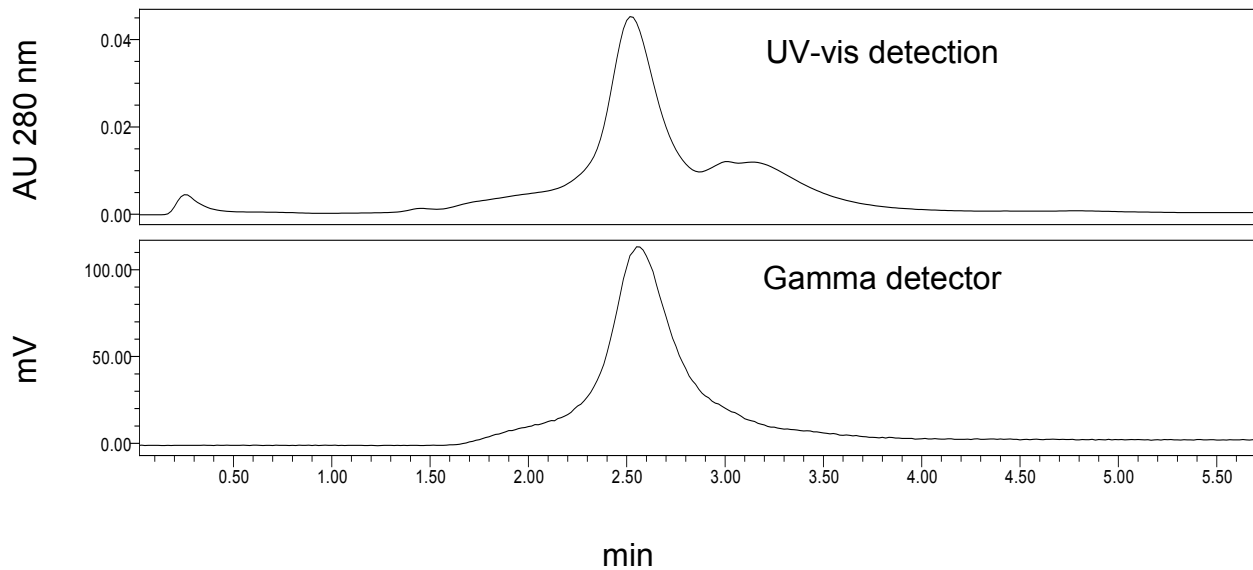
B.



C.

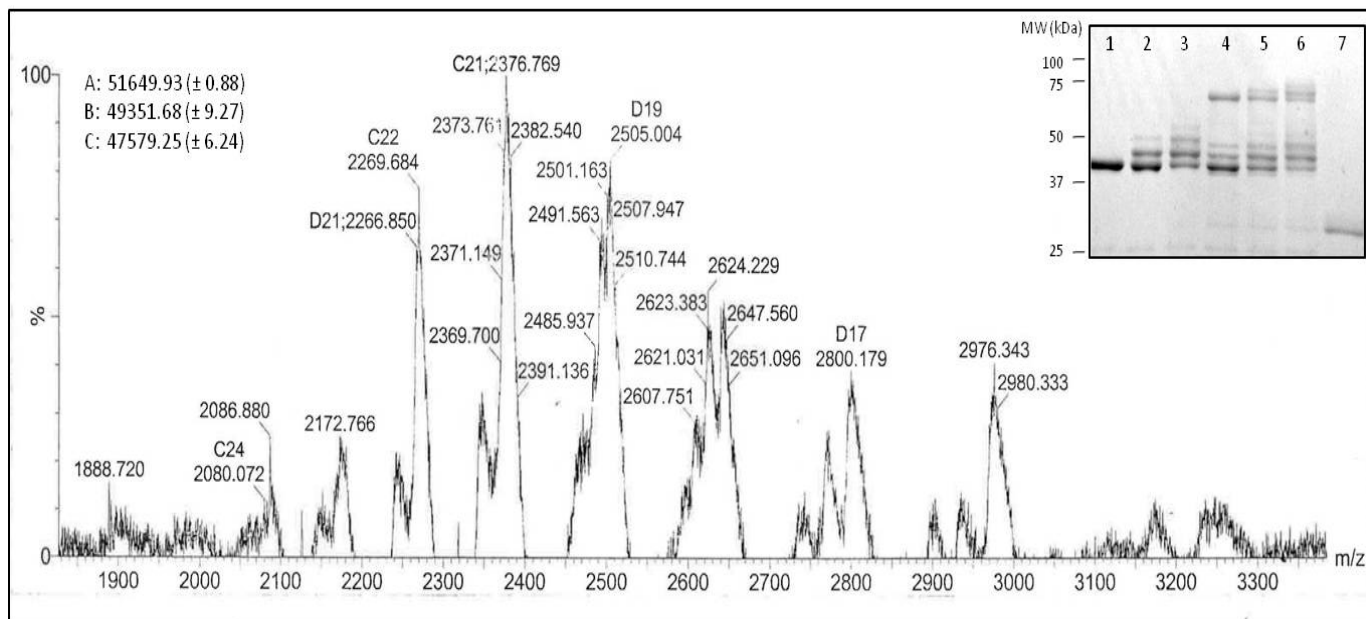


## SUPPLEMENTARY FIGURE 1



Representative HPLC analysis of  $^{123}\text{I}$ -Bn-PAI-2. A sample of purified radioiodinated protein in PBS/0.01% Tween 80 (pH 7.4) that had been stored at room temperature for 3 h was injected onto a Phenomenex Biosep 3000 column 75 x 7.5 mm and separated at a flow rate of 1.0 ml/min. Relative retention times and purity were calculated from Area Under the Curve using Empower Pro V2 (Waters) software. The major protein peak at 2.55 min in the UV-vis trace (top panel) corresponds to the radioactivity peak in the gamma detector trace (bottom panel) indicating that the majority of protein (>95%) was radiolabelled and minimal free  $^{123}\text{I}$  or radiolabelled impurities remained.

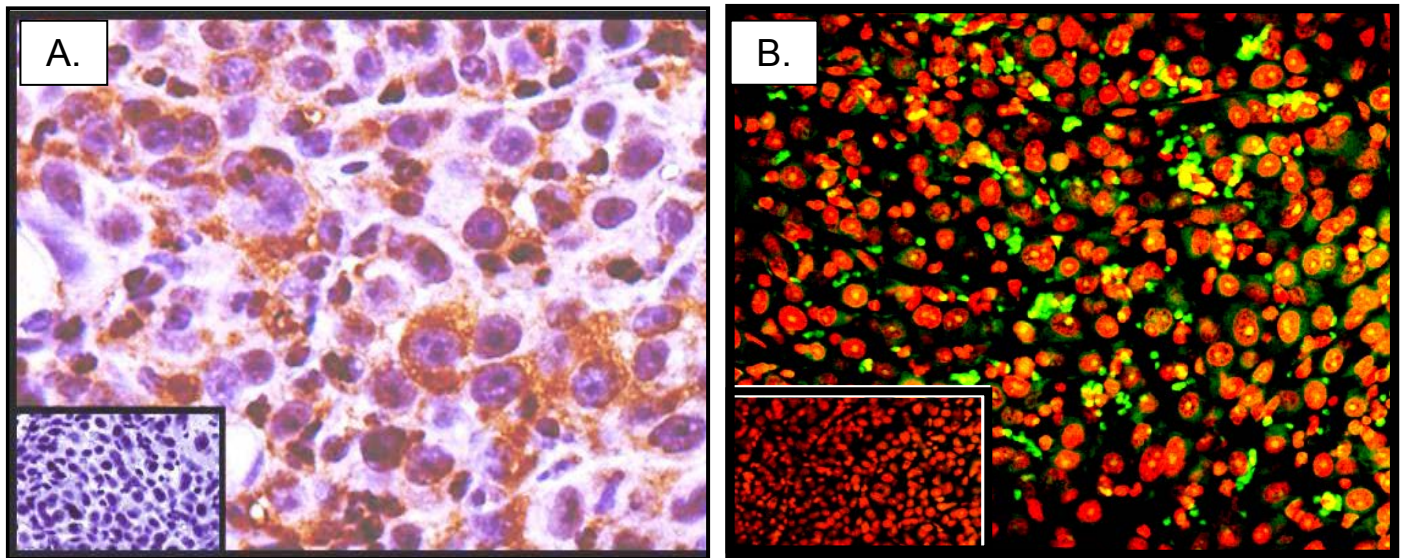
## SUPPLEMENTARY FIGURE 2



A positive ion QTOF ESI-MS of PEGylated PAI-2  $\Delta$ CD-loop in 10 mM ammonium acetate (pH 6.8) containing 0.1% formic acid. The  $m/z$  spectrum shows a Gaussian-type distribution of multiply charged ions ranging from  $m/z$  1900 – 3300. The difference in mass for each PEGylated PAI-2 species (left hand side, A - C) represents the weight of PAI-2 plus branched chain PEG ((methyl-PEO<sub>12</sub>)-PEO<sub>4</sub>, 2305.71 Da). A = mass of PAI-2 (44496.72 Da<sup>1</sup>) + 3 (methyl-PEO<sub>12</sub>)-PEO<sub>4</sub> molecules, B = mass of PAI-2 + 2 (methyl-PEO<sub>12</sub>)-PEO<sub>4</sub> molecules, C = mass of PAI-2 + 1 (methyl-PEO<sub>12</sub>)-PEO<sub>4</sub> molecule. Mass was calculated using MassLynx MS software (Waters). *Inset*: SDS PAGE of various PEGylated and non-PEGylated PAI-2  $\Delta$ CD-loop samples showing the ability of unmodified and modified PAI-2 to form stable complexes with uPA. Briefly, PAI-2  $\Delta$ CD-loop (lane 1) and PAI-2  $\Delta$ CD-loop incubated with 20-fold molar excess (methyl-PEO<sub>12</sub>)-PEO<sub>4</sub>NHS ester (lane 2) or 50-fold molar excess (methyl-PEO<sub>12</sub>)-PEO<sub>4</sub>NHS ester (lane 3) were incubated with uPA (2:1) at 37°C for 30 min. Samples were then fractionated under non-reducing conditions using 10% acrylamide SDS PAGE and visualized by staining with Coomassie blue. Both unmodified PAI-2  $\Delta$ CD-loop (lane 4) and PEGylated PAI-2  $\Delta$ CD-loop (lane 5 and 6) formed high molecular weight covalent complexes with uPA. Lane 7: uPA.

<sup>1</sup> Cochran, B. J.; Gunawardhana, L. P.; Vine, K. L.; Lee, J. A.; Lobov, S.; Ranson, M. The CD-loop of PAI-2 (SERPINB2) is redundant in the targeting, inhibition and clearance of cell surface uPA activity. *BMC Biotechnol*, **2009**, 9, 43.

### SUPPLEMENTARY FIGURE 3



Representative analysis of uPA expression in PC-3 tumour xenografts excised after BD studies by immunohistochemical (A) and immunofluorescence (B) staining of formalin-fixed paraffin embedded sections, performed essentially as previously described. Tissue sections were counterstained with either (A) Mayer's hematoxylin or (B) propidium iodide. Positive uPA staining in (A) is indicated by brown regions and in (B) by green fluorescence (orange regions indicate DNA counterstaining). **Insets:** Negative controls.